Colloids and Surfaces B: Biointerfaces 223 (2023) 113189

Contents lists available at ScienceDirect

Colloids and Surfaces B: Biointerfaces

journal homepage: www.elsevier.com/locate/colsurfb

Biomanufacturing of biomimetic three-dimensional nanofibrous multicellular constructs for tissue regeneration

Yu Zhou [a,1], Qilong Zhao [b,1,*], Min Wang [a,*]

[a] Department of Mechanical Engineering, The University of Hong Kong, Pokfulam Road, Hong Kong
[b] Institute of Biomedical and Health Engineering, Shenzhen Institute of Advanced Technology, Chinese Academy of Sciences, Shenzhen 518055, China

ARTICLE INFO

Keywords:
Biomanufacturing
Biomimetic
Electrospinning
Cell electrospraying
Tissue engineering

ABSTRACT

Biomanufacturing of functional tissue analogues is of great importance in regenerative medicine. However, this is still highly challenging due to extreme difficulties in recreating/recapitulating complicated anatomies of body tissues that have both well-defined three-dimensional (3D) multicellular organizations and bioactive nanofibrous extracellular matrix (ECM). In the current investigation, a biomanufacturing approach via concurrent emulsion electrospinning and coaxial cell electrospraying was developed, which could fabricate 3D nanofibrous multicellular constructs that resemble both the multicellular organizations and bioactive nanofibrous microenvironments of body tissues. In the proof-of-concept study, endothelial cells (ECs) and smooth muscle cells (SMCs) were placed in respective layers of multilayer-structured constructs. The two different construct layers consisted of nanofibers providing different topographies (randomly oriented nanofibers or aligned nanofibers) and contained different growth factors (vascular endothelial growth factor or platelet-derived growth factor). The ECs and SMCs in the different construct layers showed high cell densities ($> 4 \times 10^5$ cells/cm^2 after 4-day incubation) and high cell viabilities ($> 95\%$). Owing to the contact guidance/stimulation by different fibrous topographies and sequential release of different growth factors, ECs and SMCs exhibited distinct morphologies (uniformly stretched plaque-shaped or directionally elongated) and displayed enhanced proliferative activities. Our biomanufacturing approach is shown to be effective and efficient in reconstituting/replicating cell-ECM organizations as well as their interactions similar to those in body tissues such as blood vessels, indicating the great promise to produce a range of tissue analogues with biomimetic structures and functions for modeling or regenerating body tissues.

1. Introduction

Constituting/constructing body tissue analogues holds great promise for providing alternatives for organ transplantation and drug screening [1]. In recent decades, various emerging additive manufacturing techniques, such as bioprinting and electrospinning, have promoted significant progresses in this field [2–5]. However, the biomanufacturing of tissue analogues with similar structures and even functions to those of native tissue are still highly challenging [6–8]. Bioprinting has showed superiorities in preparing three-dimensional (3D) cell-laden constructs with customized shapes, biomimetic hierarchical architectures, and precisely controlled spatial patterning of multiple cell types using specifically formulated bioinks [9–11]. However, individual cells in such bioprinted constructs are usually embedded in crosslinked hydrogels, which is distinctively different from the native cell microenvironments in body tissues, i.e., cells are supported by the extracellular matrix (ECM) with nanofibrous architectures and guided by the various bioactive molecules for facilitating the interplays with cells [12,13]. Cell behaviors would therefore be restricted by the limited cell interplays, resulting in the challenge of attaining tissue-like functions for bioprinted cell-laden constructs [14]. Electrospinning is desirable in making porous scaffolds with ECM-mimetic nanofibrous architectures [15]. Electrospun scaffolds exhibit various advantages as supportive microenvironments favorable for interplays with cells and cell function determination by providing biomimetic biomechanical and biochemical guidance, respectively, through controls over the alignment of nanofibers and the encapsulation and controlled release of specific bioactive molecules [16–18]. Nevertheless, the structure of a conventional electrospun

* Corresponding authors.
E-mail addresses: ql.zhao@siat.ac.cn (Q. Zhao), memwang@hku.hk (M. Wang).
[1] These authors contributed equally to this work

https://doi.org/10.1016/j.colsurfb.2023.113189
Received 22 December 2022; Received in revised form 25 January 2023; Accepted 31 January 2023
Available online 1 February 2023

nanofibrous scaffold is normally compact and dense with nano-sized interconnected pores, allowing only very limited cell infiltration into the interior of the scaffold [19]. Although cell-laden structures can be formed by cell electrospinning [20–22], biomanufacturing multicellular constructs with precisely controlled placements of multiple types of cells within bioactive nanofibrous architectures still cannot be realized by electrospinning alone. Given that the fulfillment of tissue functions depends on both well-defined multicellular organizations and complex supportive microenvironments for offering appropriate biomechanical/biochemical cues for directing cell functions and interactions [23–25], existing biomanufacturing techniques have respective shortcomings. It is therefore highly important to develop new methods that enable the integration of well-defined multicellular organizations and bioactive nanofibrous supportive microenvironments.

Through combining bioprinting and electrospinning [26,27], it is possible to construct sandwiched cell-laden nanofibrous structures by performing bioprinting and electrospinning alternately for seeding cells and for forming nanofibrous scaffolds, respectively. Different cell types can be placed in designated positions within the nanofibrous cell-laden structures. However, in such cell-laden constructs, cells are still embedded within the bioprinted hydrogel structures. It is difficult, if possible, for the embedded cells to interact with electrospun nanofibers to take advantages of the nano-topographical cue for realizing their desired behavior and functions. Furthermore, there are obvious dimensional differences between bioprinted structs (normally, $\varphi > 500$ μm) and electrospun nanofibers (normally, $\varphi < 1$ μm), which will affect interfacial stability and also structural integrity of as-fabricated cell-laden structures. Moreover, it is very difficult to achieve the incorporation of viable cells at high densities for bioprinted cell-laden structures owing to the high shear stress during bioprinting processes, while adequate cell densities are necessary for realizing desired, biomimetic cell-cell and cell-ECM interactions [14]. Even though some advanced bioprinting techniques that use bioinks containing cell spheroids or cell-encapsulated hydrogel microparticles have been developed and shown to be capable of producing cell-laden structures with high cell densities [28–30], other problems, including the preservation of cell viability, low throughput, and technical difficulties [31], remain to integrate these techniques with electrospinning for fabricating biomimetic nanofibrous multicellular constructs.

Recently, we have demonstrated the technique of concurrent emulsion electrospinning and coaxial cell electrospraying for making cell-scaffold constructs, realizing 3D cell incorporation within bioactive

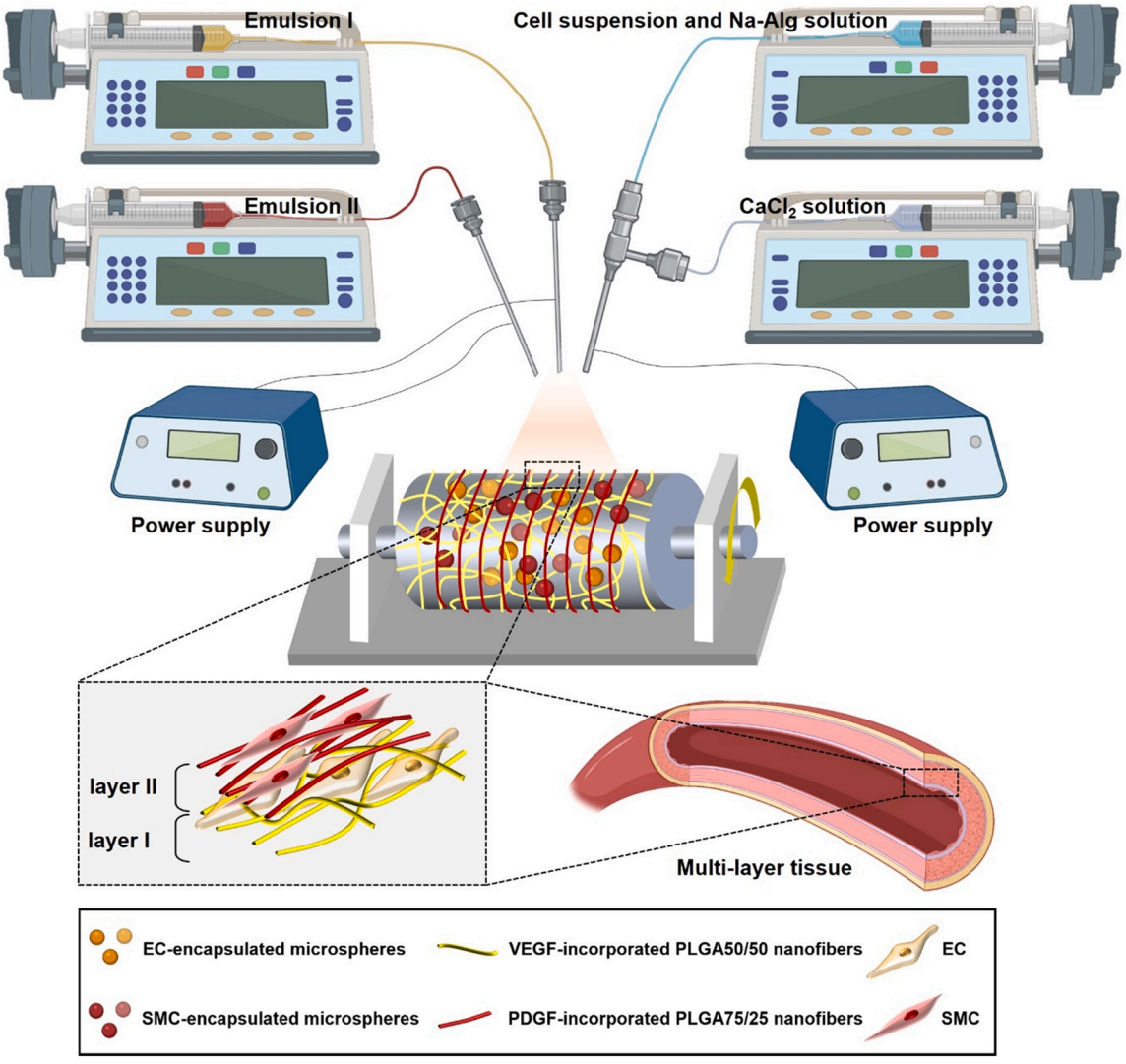

Fig. 1. Schematic diagram showing the biomanufacturing of 3D biomimetic nanofibrous multicellular constructs that resemble the anatomies of multilayered human body tissues through concurrent emulsion electrospinning and coaxial cell electrospraying, where different growth factors (VEGF and PDGF) are encapsulated in different nanofibers and different types of cells (ECs and SMCs) are placed in different construct layers consisting of either randomly oriented nanofibers or aligned nanofibers.

nanofibrous scaffolds [32]. Growth factor-incorporated nanofibers and high-density viable cells could be simultaneously deposited via concurrent emulsion electrospinning and coaxial cell electrospraying, resulting in 3D nanofibrous cell-laden structures resembling native cell-ECM organizations and interactions. Such a technique has the high potential as an alternative biomanufacturing method for fabricating cellularized constructs or tissue analogues mimicking specific anatomies, but it is unexplored so far. Guided by the anatomy of a typical multi-layered tissue, blood vessel [33], we have investigated in the current investigation biomanufacturing of 3D biomimetic nanofibrous multicellular constructs via concurrent emulsion electrospinning and coaxial cell electrospraying (Fig. 1), where endothelial cells (ECs) and smooth muscle cells (SMCs) were incorporated and placed at different layers of a scaffold that consisted of different poly(lactic-*co*-glycolic acid) (PLGA) nanofibers with different fiber arrangements (randomly oriented or aligned). Vascular endothelial growth factor (VEGF) and platelet-derived growth factor (PDGF) were encapsulated in different fibers for their local, controlled release. ECs and SMCs in the 3D nanofibrous multicellular constructs exhibited well-defined organizations, well-preserved cell viability (> 95%), and desirable cell densities (> 4 $\times 10^5$ cells/cm^2 after 4-day incubation), while cell morphologies could be determined by the topographies derived from the nanofiber arrangements and cell proliferation could be distinctively enhanced by the sequential release of different growth factors. Our biomanufacturing technique offers a promising approach for making tissue analogues that can mimic the natural cell-cell and cell-ECM organizations and interactions, which opens a new avenue for engineering cellularized constructs for tissue repair and for building tissue models for drug screening.

2. Materials and methods

2.1. Materials

Two types of medical grade PLGA with the LA:GA molar ratio of 50:50 (PLGA50/50, average Mw: 120,000) and 75:25 (PLGA75/25, average Mw: 120,000), respectively, were purchased from Lakeshore Biomaterials, USA, and used for fabricating different layers of 3D nanofibrous multicellular constructs. Sodium alginate (Na-Alg), calcium chloride ($CaCl_2$), sodium citrate (Na-citrate), trifluoroethanol (TFE), sodium azide, bovine serum albumin (BSA), Tween-20 and tablets for making phosphate buffer saline (PBS) were products of Sigma-Aldrich, USA. VEGF (recombinant human $VEGF_{165}$), PDGF (recombinant human PDGF-BB) and corresponding enzyme-linked immunosorbent assay (ELISA) kits (human $VEGF_{165}$ standard ABTS ELISA development kits and human PDGF-BB standard ABTS ELISA development kits) were products of PeproTech Inc., USA. LIVE/DEAD viability kits containing calcein acetoxymethylester (Calcein-AM) and ethidium homodimer-1 (EthD-1), CellTracker™ Orange CMRA, Alexa Fluor 488 Phalloidin, and 4′,6-diamidino-2-phenylindole (DAPI) for cell staining were supplied by Invitrogen, UK. Deionized water (DI water) was produced by a DI water producer (Model D12681, Barnstead International, USA).

2.2. Cell culture

Primary human umbilical vein endothelial cell (HUVEC) and primary human aortic smooth muscle cell (HASMC), both provided by Life Technologies, USA, were respectively used as model EC and SMC in the current investigation. HUVECs were expanded in an EC-specific cell culture medium (M200, Life Technologies, USA) with supplemented 2 v/v% low serum growth supplement (Life Technologies, USA), 100 units/mL penicillin-streptomycin (Life Technologies, USA), and 4 μg/mL fungizone (Life Technologies, USA). HASMCs were expanded in an SMC-specific cell culture medium (M231, Life Technologies, USA) with supplemented 2 v/v% smooth muscle growth supplement (Life Technologies, USA), 100 units/mL penicillin-streptomycin (Life Technologies, USA), and 4 μg/mL fungizone (Life Technologies, USA). Both types of cells were maintained in a humidified cell culture incubator (37 °C, 5 v/v% CO_2) and trypsinized at 70% cell confluence for preparing cell suspensions.

2.3. Biomanufacturing of cell-scaffold constructs

Prior to the biomanufacturing of 3D nanofibrous multicellular constructs, the polymers (PLGA50/50, PLGA75/25, and Na-alginate) and reagents ($CaCl_2$, TFE, and Na-citrate) to be used were sterilized by γ-ray radiation using a Cobalt 60 source at an intensity of 15 kGy for 30 mins. Concurrent emulsion electrospinning and coaxial cell electrospraying for making 3D nanofibrous multicellular constructs was performed in a Class II, type A laminar flow culture hood following the established procedures [32]. Briefly, for producing the first layer in the constructs where HUVECs were incorporated within VEGF-loaded and randomly oriented nanofibrous matrix, electrospinning of an emulsion prepared by mixing a PLGA50/50 solution (20 w/v% in TFE) and a VEGF-containing PBS (10 mg/mL) at the volume ratio of 10:1 under mechanical stirring and electrospraying using a coaxial spinneret with the inner and outer nozzles fed respectively with a supplemented HUVEC suspension (cell density: 5 $\times 10^6$ cells/mL, supplemented with 4 w/v% Na-Alg) and a $CaCl_2$ aqueous solution (1.5% w/v) were performed simultaneously, aiming to co-deposit VEGF-loaded PLGA50/50 electrospun nanofibers and HUVEC-encapsulated and calcium-ion-crosslinked alginate hydrogel (Ca-Alg) microspheres on a rotating collection drum at a low-speed rotation (30 rpm), with the HUVEC-containing microspheres being evenly distributed among randomly oriented VEGF-loaded nanofibers. After 1-h co-deposition, the electrospinning side was switched to using an emulsion containing 20 w/v% PLGA75/25 and suspended PDGF. At the same time, the inner flow of the coaxial cell electrospraying side was switched to using a supplemented HASMC suspension (cell density: 5 $\times 10^6$ cells/mL, supplemented with 4 w/v% Na-Alg). Therefore, emulsion electrospun PDGF-loaded PLGA75/25 nanofibers and electrosprayed HASMC-encapsulated Ca-Alg microspheres were co-deposited for 1 h onto the first layer on the collection drum which now rotated at a high speed (3000 rpm), with the high rotation speed being used for aligning the electrospun nanofibers. The resulting cell-laden bilayer structures were then immersed in 0.055 M Na-citrate-containing PBS for 30 min for selectively breaking up the Ca-Alg microspheres and therefore releasing the encapsulated cells, finally resulting in the 3D multicellular constructs as designed for the current investigation.

2.4. Morphological and structural characterizations

The biomanufactured 3D multicellular constructs were freeze-dried and sputtered with a thin layer of gold. They were then examined under a field emission scanning electron microscope (SEM, LEO 1530, Germany) from their top, bottom, and cross sections. The thickness and the interface between the two layers in the constructs were investigated through the cross-sections. The morphologies of these two layers were viewed from the bottom and from the top, respectively. Average diameters (φ) of the emulsion electrospun VEGF-loaded PLGA50/50 fibers and PDGF-loaded PLGA75/25 fibers were statistically analyzed ($N > 50$) with the assistance of the ImageJ software (https://imagej.nih.gov/ij/).

2.5. In vitro growth factor release studies

For assessing the in vitro release behavior of VEGF and PDGF, bilayer scaffolds consisting of one layer of VEGF-loaded PLGA50/50 nanofibers and one layer of PDGF-loaded PLGA75/25 nanofibers were produced through emulsion electrospinning using the same fabrication procedure (but minus electrospraying) and the same processing parameters as those used in the biomanufacturing process but without incorporating

the cells. As-fabricated bilayer scaffolds were then cut into pieces, weighed, and immersed in 37 °C medium supplemented with 0.02% w/v sodium azide (for the antibacterial purpose), 0.05% v/v Tween-20 (for reducing nonspecific protein absorption) and 0.5% w/v BSA (for stabilizing the released growth factor). At pre-determined time points, the immersion medium was collected and refreshed. The contents of different growth factors, i.e., VEGF and PDGF, were detected using corresponding ELISA kits and their amounts were measured using a microplate reader (UVM 340, Asys HiTech GmbH, Australia) at the wavelength of 405 nm with a reference wavelength of 650 nm. Cumulative release curves for VEGF and PDGF, respectively, were then plotted ($N = 6$).

2.6. Cell distribution examination

For examining distributions of HUVECs and HASMCs within 3D multicellular constructs, HUVEC- or HASMC-incorporated monolayer constructs were firstly prepared. The encapsulated cells in Ca-Alg microspheres within monolayer constructs and the released cells within the fibrous matrix after the immersion treatment in Na-citrate solution were stained by Calcein AM, and their distributions were observed under a fluorescence microscope (Ti-U, Nikon, Japan). Afterwards, 3D multicellular constructs were fabricated using HUVECs and HASMCs pre-stained with Calcein-AM and CellTracker™ Orange CMRA, respectively. The z-axis distributions of different types of cells across the thickness of 3D multicellular constructs were examined by using a laser scanning confocal microscope (LSCM, LSM710, Carl Zeiss, Germany).

2.7. Cell viability assessment

For HUVEC- or HASMC-incorporated monolayer constructs produced by concurrent emulsion electrospinning and coaxial cell electrospraying (at either low or high rotational speed for the rotating collection drum), encapsulated cells in Ca-Alg microspheres within the monolayer constructs and released cells in the nanofibrous matrix after the immersion treatment in Na-citrate solution were stained with a H_2O_2-sensitive fluorophore, dichlorofluorescein diacetate (DCFDA), and DAPI for probing the intracellular reactive oxygen species (ROS) level, or stained by using the LIVE/DEAD viability kit according to the manufacture's protocol. The sample were subsequently observed under the fluorescence microscope for assessing cell viability.

2.8. Immunochemical staining for cells and cell distribution

After 4-day incubation of 3D multicellular constructs (with growth factor-free constructs being made and used as controls) in the combined medium which was made by mixing the supplemented M200 and supplemented M231 at the volume ratio of 1:1, both HUVECs and HASMCs within the constructs were fixed with 4 v/v% paraformaldehyde, treated with PBS with additions of 1 w/v% BSA and 0.1 v/v% Tween 20 for permeabilization and blocking, stained with Alexa Fluor 488 Phalloidin and DAPI, respectively, for labeling actin filaments (F-actin) and nucleus according to the manufacturer's protocol and kept at 4 °C overnight, and finally observed under LSCM. The orientation, density and cell area fraction of HUVECs and HASMCs in the different layers of 3D multicellular constructs were statistically analyzed using LSCM images obtained from the experiments.

2.9. Cell proliferation

For quantitatively comparing the viability and proliferation of different cell types in 3D fibrous constructs over the incubation period, cells in cultured monolayer cell-incorporated constructs after 1-, 4- and 7-day incubation times were stained with 3-(4,5-dimethylthiazol-2-yl)− 2,5-diphenyltetrazolium bromide (MTT, Sigma-Aldrich, USA). Samples for MTT assay were incubated with a MTT working solution at 37 °C for 4 h. The working solution was then removed carefully. The formazan formed were dissolved by 300 μL dimethyl sulfoxide (Sigma-Aldrich, USA) under slight shaking for 10 mins., where the optical density (O.D.) value of each sample was determined using the microplate reader at the measuring wavelength of 570 nm.

2.10. Statistics

All numerical data in this study were expressed as means ± standard deviation. Statistical analysis was performed using analysis of variance (ANOVA) with unpaired Student's t tests. Nonsignificant (n.s.) states no statistically significant difference, while *$P < 0.05$ and * *$P < 0.01$ were considered statistically significant.

3. Results

3.1. Biomanufacturing of 3D biomimetic nanofibrous multicellular constructs

Many human body tissues have complex, multilayered tissue structures [24]. For example, blood vessels exhibit a multilayered structure in which the inner endothelium and the medium smooth muscle layers contribute to their main functions such as barrier and systolic/diastolic functions [34]. The endothelium and smooth muscle layers show distinctly different anatomies. While the endothelium consists of a confluence EC layer with the tight intercellular junctions among plaque-shaped ECs supported by VEGF-releasing nanofibrous ECM [35], the smooth muscle layers show specific arrangements of SMCs (inner circular layer and outer longitudinal layer) with parallel, aligned cells of a certain orientation supported by PDGF-releasing nanofibrous ECM in each layer [36]. For the biomanufacturing of 3D nanofibrous multicellular constructs with a vessel-mimicking bilayer structure, where ECs and SMCs (herein using HUVECs and HASMCs as their respective models) and different growth factors (VEGF and PDGF) were placed in different polymeric nanofibrous layers (PLGA50/50 and PLGA75/25) with distinct arrangements (randomly oriented and aligned) of nanofibers, this concurrent emulsion electrospinning and coaxial cell electrospraying approach with adaptions was applied (Fig. 1). The rotational speed of the rotating collection drum was changed from 30 to 3000 rpm during sequential productions of the two layers, leading to different fibrous architectures in different layers: random fiber orientations from a low (i.e., 30 rpm) rotational speed and aligned fibers from a high (i.e., 3000 rpm) rotational speed. Different types of cells were encapsulated in Ca-Alg microspheres through coaxial cell electrospraying, which were embedded in emulsion electrospun growth-factor-loaded nanofibers during the co-depositions processes. Subsequently, the cells were released from Ca-Alg microspheres and hence distributed in the nanofibrous matrix after the immersion treatment in a Na-citrate solution, presenting 3D biomimetic nanofibrous multicellular constructs for applications in regenerative medicine.

In one set of experiments, throughout the biomanufacturing process, cells were stained with Calcein-AM (only staining viable cells) for tracking their distributions in biomanufactured 3D biomimetic nanofibrous multicellular scaffolds/constructs. The distributions of cells in different individual layers using monolayer constructs were firstly investigated. Prior to the immersion treatment in a Na-citrate solution of the HUVEC-incorporated constructs, HUVEC-encapsulated microspheres with diameters ranging from 100 to 200 μm were found to be evenly dispersed in the fibrous matrix of randomly oriented nanofibers (Fig. 2a). After the immersion treatment, Ca-Alg microspheres completely disappeared, leaving the stained HUVECs randomly distributed within the fibrous matrix of the constructs (Fig. 2a). Similarly, HASMC-encapsulated microspheres were also seen to be evenly distributed in the fibrous matrix of HASMC-incorporated constructs consisting of aligned nanofibers (Fig. 2b), where encapsulated HASMCs could be successfully released and randomly distributed in the aligned-

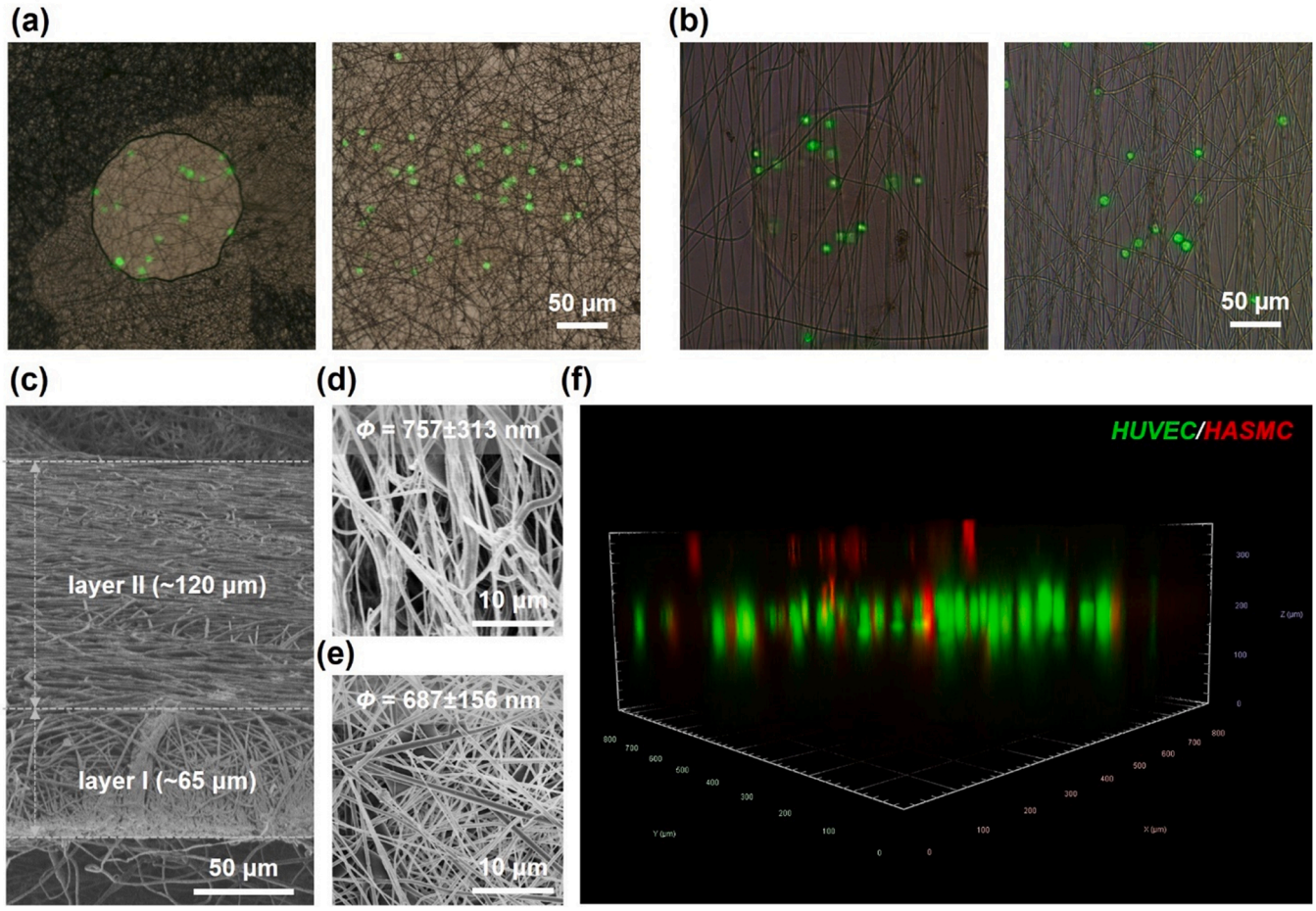

Fig. 2. Formation of 3D biomimetic nanofibrous multicellular constructs: (a) Formation of the first layer of 3D biomimetic nanofibrous multicellular constructs with the incorporation of ECs (labelled by Calcein AM) in the matrix of randomly oriented nanofibers before (left) and after (right) cell release through break-up of Ca-Alg hydrogel microspheres. (b) Formation of the second layer of the 3D biomimetic nanofibrous multicellular constructs with the incorporation of SMCs (labelled by Calcein AM) in the matrix of aligned nanofibers before (left) and after (right) cell release through break-up of Ca-Alg hydrogel microspheres. (c) A cross-sectional view of the bilayer structure of 3D biomimetic nanofibrous multicellular constructs. (d) Morphology (top view) of the second construct layer consisting of aligned nanofibers. (e) Morphology (top view) of the first construct layer consisting of randomly oriented nanofibers. (f) A representative LSCM image showing distributions of HUVECs (labelled by Calcein AM in green) and HASMCs (labelled by CellTracker™ Orange CMRA in red) across the *z*-axis of 3D biomimetic nanofibrous multicellular constructs.

fiber matrix after breaking up of Ca-Alg microspheres by the immersion treatment with a Na-citrate solution (Fig. 2b). These results have shown that both viable HUVECs and viable HASMCs could be incorporated uniformly in the fibrous matrix of different construct layers with either randomly oriented nanofibers or aligned nanofibers.

3D biomimetic multicellular constructs were eventually made through biomanufacturing as described. The 3D multicellular constructs exhibited clear bilayer structures (Fig. 2c), with a bottom layer (layer I) having a thickness of about 65 μm and an upper layer (layer II) having a thickness of about 120 μm. The larger thickness for the upper layer consisting of PLGA75/25 nanofibers than the bottom layer consisting of PLGA50/50 nanofibers, which was formed using the same manufacturing duration (i.e., 1 h), could be attributed to the electrostatic repulsion effect. In the situation that the same thickness is desired for both layers, the electrostatic repulsion effect can be dealt with through the alternate use of positive- and negative-voltage electrospinning [37]. Notably, nanofibers in the two layers exhibited different arrangements: aligned and densely packed PLGA75/25 nanofibers with an average fiber diameter of 757 ± 313 nm in the upper layer of the constructs (Fig. 2d), and randomly oriented PLGA50/50 nanofibers with an average fiber diameter of 687 ± 156 nm are in the bottom layer of the constructs (Fig. 2e). HUVECs and HASMCs were labeled with Calcein-AM and CellTracker™ Orange CMRA, respectively, and their distributions within the constructs were examined. It could be seen clearly that a bilayer distribution of different cell types in the *z*-axis across the thickness (~200 μm) of constructs exited (Fig. 2f), indicating successful formation of 3D nanofibrous multicellular constructs with biomimetic organizations of ECs and SMCs. In addition, owing to similar throughputs between emulsion electrospinning (3.0 mL/h) and coaxial cell electrospraying (2.0 mL/h), as well as relatively small sizes of cell-encapsulated Ca-Alg microspheres, the biomanufactured 3D nanofibrous constructs exhibited desirable structural integrity and also uniform distributions of different cell types in different layers.

3.2. *Influence of the biomanufacturing process on cell viability*

Given the formation of 3D nanofibrous multicellular constructs through current concurrent electrospinning and electrospraying approach involved high voltage, high-speed rotation and the post-electrospraying treatment with a dilute Na-citrate solution, it was therefore very important to investigate specific influences, if any, of the biomanufacturing process on the viability of cells within the constructs. To assess cell viability, HUVEC-incorporated constructs with randomly oriented nanofibers and HASMC-incorporated constructs with aligned nanofibers were made separately, and the incorporated cells were stained with a H_2O_2-sensitive fluorophore, DCFDA, and a LIVE/DEAD

viability kit. High levels of ROS have been proven to be an indicator of cellular damage and are linked to cell apoptosis [38]. Through staining HUVECs (the released cells) with DCFDA within fibrous scaffolds formed by the current biomanufacturing process and comparing their results with those of cells manually seeded onto emulsion electrospun PLGA50/50 nanofibrous scaffolds (which were the control), it was observed that there was no significant difference between the released cells and cells in the control in either the percentage (both about 10%) of cells with high intracellular ROS levels with respect to the total cell number (labelled by DAPI) or the fluorescence intensity relevant to the amount of intracellular ROS (Fig. 3a). These results indicated that there was no obvious cell damage that could be potentially made by the current biomanufacturing process. Though the concurrent biomanufacturing potentially involved the evaporation of organic solvents that might be toxic to cells, the cytocompatibility results confirmed that the microencapsulation of cells within the Ca-Alg hydrogel microspheres was effective to offer the protective capsular microenvironments that barriered the potential harm to the encapsulated cells. After biomanufacturing and subsequent 1-day culture, the viability of released HUVECs and that of cells in the control were also compared: both cells exhibited high viability (> 96%) (Fig. 3b). The viability of HUVECs incorporated in PLGA50/50-based constructs did not show statistically significant difference to that of HUVECs directly seeded on emulsion electrospun PLGA50/50 nanofibrous scaffolds (Fig. 3c).

As for HASMC-incorporated constructs, even though high-speed rotation which may cause high shear stress to cells was additionally used, the intracellular ROS level of HASMCs released from Ca-Alg microspheres after immersion treatment with a dilute Na-citrate solution and distributed in the PLGA75/25 nanofibrous scaffolds were not obviously raised when compared to the control group (i.e., HASMCs manually seeded onto emulsion electrospun PLGA75/25 nanofibrous scaffolds) (Fig. 3d). HASMCs incorporated in PLGA75/25-based constructs of aligned nanofibers could also maintain a desirable cell viability (> 95%) after the biomanufacturing process and subsequent 1-day culture (Fig. 3e), showing no statistically significant difference as compared to the control (Fig. 3f). These results revealed that both HUVECs and HASMCs could preserve high cell viability within the nanofibrous matrix of constructs formed by the current biomanufacturing process whether or not it involved high-speed rotation for construct fabrication, offering great prospect for fulfilling the biomimetic functions and promoting interactions of cells within 3D nanofibrous multicellular constructs.

3.3. *Behavior and functions of different cell types within biomanufactured 3D nanofibrous multicellular constructs*

For human body tissues and organs, their functions are usually realized by programming the behavior and functions of the constituting multiple types of cells through specific cell-cell and cell-ECM interactions [39]. The secretions of soluble bioactive biomolecules, e.g., growth factors, are important communication means for promoting cell-cell and cell-ECM interactions [40], which are essential for tissue regeneration. For example, VEGF and PDGF play important roles in mediating vascular regeneration. Notably, VEGF and PDGF are secreted and activated sequentially at different stages of vascular regeneration: firstly the initiation of endothelium remodeling mediated by VEGF, and later the stimulation of smooth muscle maturation by PDGF [41]. In addition to mimicking the layered organizations of ECs and SMCs within nanofibrous matrix of blood vessels, the biomanufactured constructs were loaded with VEGF and PDGF in respective nanofibers of different construct layers through emulsion electrospinning to mimic the bioactivities of native environments of blood vessels. To render the loaded VEGF and PDGF for sequential release in specific spatiotemporal manners so as to meet in-service requirements, two polymers, PLGA50/50 and PLGA 75/25, which have different biodegradation rates [42], in the same PLGA family were chosen to form emulsion electrospun nanofibers

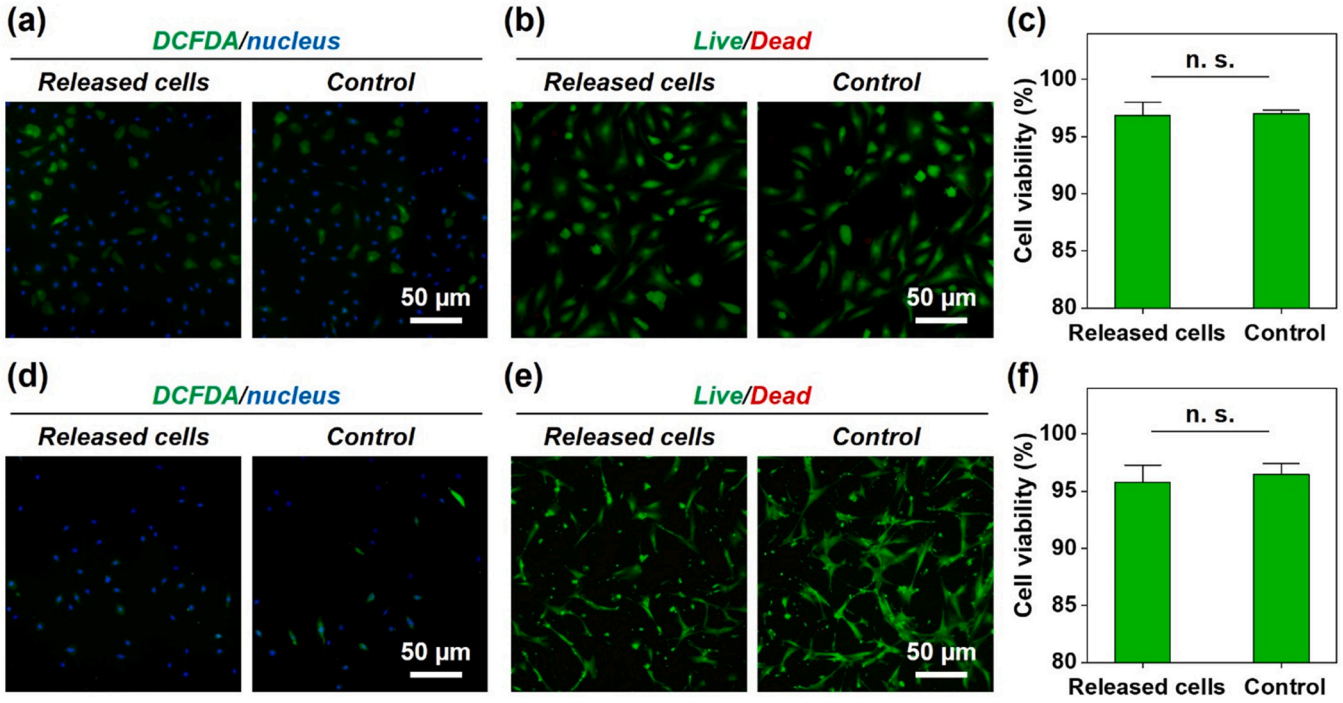

Fig. 3. Cell viability throughout the biomanufacturing process of concurrent emulsion electrospinning and coaxial cell electrospraying with the immersion treatment in a dilute Na-citrate solution: (a) Comparison of intracellular ROS levels between HUVECs incorporated in nanofibrous scaffolds through biomanufacturing (Released cells) and HUVECs on nanofibrous scaffolds through manual cell seeding (Control). (b, c) Comparison of cell viability between released HUVECs in biomanufactured constructs and manually seeded HUVECs in the control. (d) Comparison of intracellular ROS levels between HASMCs incorporated in nanofibrous scaffolds through biomanufacturing (Released cells) and HASMCs on nanofibrous scaffolds through manual cell seeding (Control). (e, f) Comparison of cell viability between released HASMCs in biomanufactured constructs and manually seeded HASMCs in the control. (n. s.: no statistically significant difference.).

as the delivery vehicles for VEGF and PDGF, respectively. Owing to thinner diameters and higher degradation rates of emulsion electrospun PLGA50/50 nanofibers than those of the PLGA75/25 nanofibers, the release of growth factors, where molecular diffusion of growth factors depends on the swelling and biodegradation of specific polymeric nanofibers [43], from PLGA50/50 nanofibers would be faster than that from PLGA75/25 nanofibers (Fig. 4a). Sequential releases of VEGF and PDGF from their own layers of 3D nanofibrous multicellular constructs, which would accommodate in-service spatiotemporal delivery requirements, were therefore realized.

The behavior and functions of different types of cells (HUVECs and HASMCs) incorporated in different layers of 3D nanofibrous multicellular constructs, which were guided by both the topography of nanofibrous architecture and sequential release of different growth factors, were systematically investigated. Compared to cells in growth factor-free constructs (*VEGF-* and *PDGF-* samples) after culturing for 4 days, both HUVECs and HASMCs exhibited significantly enhanced cytoskeleton developments with sufficiently stretched cell morphologies and larger numbers of cells, respectively, in the layers of constructs loaded with VEGF and PDGF (*VEGF+* and *PDGF+* samples) (Fig. 4b, 4c). In the HUVEC-incorporated layer with or without the loading of VEGF, cells showed plaque shapes without specific orientation in cell morphology (Fig. 4d), which was mainly determined by the arrangement of nanofibers that were randomly orientated. The sustained release of VEGF enhanced cytoskeleton development and proliferation of the incorporated HUVECs, with more than two-folds of cell density (Fig. 4e) and nearly three-folds of cell area fraction (Fig. 4f) being observed for HUVECs in the VEGF-loaded layer as compared to HUVECs in the VEGF-free layer. It should be noted that the density of HUVECs had reached 4×10^5 cells/cm^2 in the VEGF-loaded layer of constructs biomanufactured in the current investigation, which was higher than that in normal bioprinted structures [14]. Furthermore, since cells in the

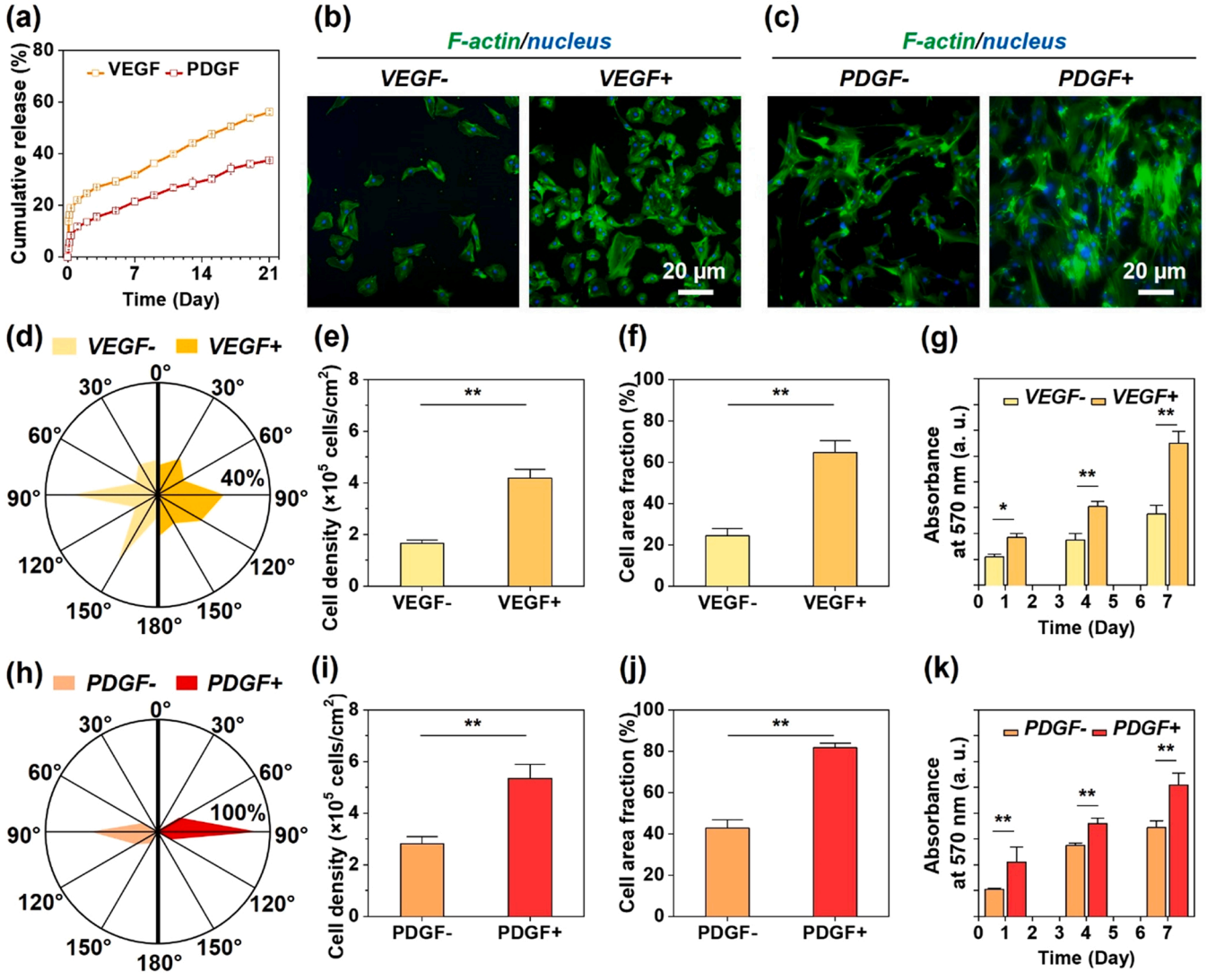

Fig. 4. Bioactivities of 3D biomimetic nanofibrous multicellular constructs: (a) *In vitro* release profiles of VEGF and PDGF from the different layers of 3D biomimetic nanofibrous constructs within the test period of 21 days. (b) Cytoskeleton organization of HUVECs in the nanofibrous layer without (*VEGF-*) or with (*VEGF+*) VEGF loading. (c) Cytoskeleton organization of HASMCs in the nanofibrous layer without (*PDGF-*) and with (*PDGF+*) PDGF loading. (d) Analysis of the orientation of cell morphology for HUVECs in the randomly oriented nanofibrous constructs. (e) Comparison of cell density of HUVECs between *VEGF-* and *VEGF+* nanofibrous layers after 4-day cell culture. (f) Comparison of cell area fraction of HUVECs between *VEGF-* and *VEGF+* nanofibrous layers after 4-day cell culture. (g) Comparison of cell proliferation of HUVECs between *VEGF-* and *VEGF+* nanofibrous layers within the cell culture period of 7 days through MTT assay. (h) Analysis of the orientation of cell morphology for HASMCs in the aligned nanofibrous constructs. (i) Comparison of cell density of HASMCs between *PDGF-* and *PDGF+* nanofibrous layers after 4-day cell culture. (j) Comparison of cell area fraction of HASMCs between *PDGF-* and *PDGF+* nanofibrous layers after 4-day cell culture. (k) Comparison of cell proliferation of HASMCs between *PDGF-* and *PDGF+* nanofibrous layers within the cell culture period of 7 days through MTT assay. (*P < 0.05. **P < 0.01.).

current 3D constructs were distributed in the nanofibrous matrix, which had space for cell spreading and morphogenesis, rather than embedded in a bioprinted hydrogel structure, which restricted/immobilized cells, the HUVECs in the constructs exhibited desirable proliferative activities with increasing cell numbers over time within the culture period of 7 days (Fig. 4g). The loading and subsequently sustained release of VEGF from the nanofibrous matrix further enhanced the spreading and proliferation of HUVECs, which were consistent with the results obtained by others in previous studies that demonstrated the stimulating effects of VEGF on the functions (including survival, proliferation, migration, and tubulogenesis) of endothelial cells by initiating complex networks of signaling pathways via the activations of multiple receptors (e.g., kinase-insert-domain-containing receptor. phospholipase C-γ, protein kinase C, extracellular-signal-regulated protein kinase, focal adhesion kinase) [44]. The results also indicated attractive potential of generating sufficient cell-cell interactions to form a confluence EC monolayer for endothelialization after 3D cell culture [45]. As for the HASMC-incorporated layer, HASMCs in the nanofibrous layer showed obvious elongated cell morphology, with a certain induced orientation (more than 90% of cells oriented in the direction ranging from 60° to 120°) regardless of the loading condition for PDGF (*PDGF*+ or *PDGF*-) (Fig. 4c, 4h), mimicking the anatomies of smooth muscle layers in the blood vessel [36]. In addition, the sustained release of PDGF effectively promoted the cytoskeleton development and proliferation of HASMCs in the PDGF-loaded nanofibrous layer, as evidenced by the results of comparative studies in cell density (Fig. 4i), cell area fractions (Fig. 4j) and MTT assay (Fig. 4k). PDGF has been proven to be critical in mediating the proliferation of vascular smooth muscle cells via receptor tyrosine kinase signaling [46]. Accordingly, we could observe enhanced cytoskeleton development and proliferative activity of HASMCs owing to the sustained release of PDGF, which would impart sufficient cell-cell interactions among cells and subsequently promote the maturation of SMCs, potentially facilitating the functional restoration of smooth muscle layers in blood vessels [47]. The above results indicated that 3D nanofibrous multicellular constructs made in the current investigation could support the growth and cell-cell interactions for both HUVECs and HASMCs in their bioactive nanofibrous matrix in the 3D cell culture condition. The behavior and functions of HUVECs and HASMCs could be further guided by the topography and sequential release of multiple growth factors, mimicking the natural cell-ECM interactions.

4. Discussion

Tissue regeneration holds great promise in treating the injuries, losses, dysfunctions, or diseases of body tissues and organs, however, it remains extremely challenging owing to the high complexity in the architectures and organizations of native body tissues/organs. In general, body tissues/organs consist of multiple cells, where different types of cells are located at designated positions and supported by nanofibrous ECM. Cell-ECM interactions (directing cellular functions by specific biomechanical and biochemical cues of ECM) and cell-cell interactions (directing cellular functions by the communications among the multiple types of cells) work together to determine the tissue functions and regeneration. Consequently, it would be highly promising for directly assisting tissue regeneration or investigating the underlying mechanisms if we could manufacture the tissue analogues that contain well-defined multiple cells and nanofibrous supportive microenvironments and reconstitute/recapitulate the natural cell-ECM and cell-cell interactions.

Emerging biomanufacturing techniques, e.g., bioprinting [9–11] and electrospinning [16–18], have been developed and studied for fabricating such constructs of tissue analogues, however, respective limitations remain. Despite excellent versatility of bioprinting in making multicellular constructs with well-defined organizations of multiple types of cells, bioprinted cell-laden structures usually lack biomimetic nanofibrous architectures as supportive microenvironments, which would affect the reconstruction of biomimetic cell-EC interactions. In contrast, electrospinning is effective to form bioactive nanofibrous constructs which resemble the nanofibrous architecture of ECM but cannot place different types of cells into designated 3D positions in the constructs to mimic the natural multicellular organizations and cell-cell interactions. To the best of our knowledge, up to our current investigation, there has been no fabrication technique reported in the open literature that enables integrated manufacturing of 3D nanofibrous multicellular constructs mimicking multilayered tissue structures such as natural blood vessels which exhibit both bioactive nanofibrous architectures and well-defined multicellular organizations. Recently, we demonstrated the concurrent emulsion electrospinning and coaxial cell electrospraying approach that is effective and efficient in forming 3D bioactive nanofibrous cell-laden structures [32], providing the promise of biomanufacturing 3D biomimetic nanofibrous multicellular constructs that can be superior as new tissue analogues for better recapitulating/replicating natural cell-ECM organizations and interactions in body tissues such as blood vessels. Inspired by the established research, the biomanufacturing approach demonstrated in the current investigation succeeded to effectively and efficiently fabricate 3D nanofibrous multicellular constructs with the organizations and interplays between cells (ECs and SMCs) and the bioactive nanofibrous matrix (VEGF-loaded randomly oriented nanofibers and PDGF-loaded aligned nanofibers) that mimic both natural cell-cell interactions and cell-ECM interactions in blood vessels, addressing the challenges that existing biomanufacturing techniques have faced.

Through concurrent emulsion electrospinning and coaxial cell electrospraying, the constructs mimicking the anatomies of blood vessels in terms of both their multicellular organizations and nanofibrous bioactive supportive microenvironments were successfully formed, holding great promise to engineering vascular models for cell biology investigations, drug testing, and regenerative medicine applications. In the endeavor of reconstituting/replicating the complicated structures and functions of blood vessels, the biomimicry of endothelial glycocalyx layer (EGL), a thin layer (~500 nm) consisting of glycoproteins and glycosaminoglycan on the luminal surface of blood vessels and essential in modulating inflammation response, vascular permeability, and mechanotransduction of endothelial cells [48], has also attracted increasing interests. The EGL exhibits brush-like nano-filamentous (~20 nm) supramolecular architectures, containing a net negative charge owing to the polyanionic compositions. The net negative charge contributes to their functions of binding of enzymes, enzyme inhibitors, growth factors, and cytokines via electrostatic interactions. Although the recreation of the ultrathin nano-filamentous structures of EGL can be challenging for existing engineering methods, at least its partial functions may be mimicked as we have already shown a method of negative-voltage emulsion electrospinning [49], which enabled the formation of electrospun nanofibers with net negative charges and thereby controlled releases of angiogenic factors mediated by electrostatic interactions. It can be postulated that the supramolecular architectures, functions, and even the interplays with endothelial cells of the endothelial glycocalyx layer can further be reconstituted/replicated through the integration of multiple techniques such as the established concurrent biomanufacturing, negative-voltage electrospinning, and molecular self-assembly.

For the concurrent biomanufacturing method, one major concern is whether the viability and functions of the cells would be impaired by the manufacturing process that involved high voltage, the evaporation of organic solvents during the concurrent emulsion electrospinning, and high-speed rotation of the collector when making the layer made of parallel aligned nanofibers. Since the coaxial cell electrospraying was performed at an electrostatic field, the cells within the electrosprayed microspheres would not be affected because there would be negligible electrical gradients and currents passing through the cells with small diameters (ranging 5–20 μm) [22]. Our previous study also confirmed that the evaporation of organic solvents during the concurrent emulsion electrospinning process would not affect the viability of cells that were

encapsulated within the protective hydrogel microspheres [32]. The shear stress generated along with the high-speed rotation of the collector might be a potential threat to cell viability. However, the microspheres formed along with the parallel aligned nanofibers showed few differences in structure compared to those formed along with the randomly oriented nanofibers (Fig. 2a, 2b). The results inferred that there was insignificant stretch exerted on the cell-encapsulated microspheres by the shear stress during the concurrent formation of the parallel aligned nanofibers. To verify the technical feasibility and safety, we have performed detailed investigations into the potential influence on the cellular viability at molecular (intracellular ROS level) and cellular (LIVE/DEAD viability staining assay) levels. The results indicated that the viability of cells would be not affected in the concurrent biomanufacturing process, regardless of simultaneously performing with emulsion electrospinning at either low-speed (Fig. 3a-3c) or high-speed (Fig. 3d-3f) rotation modes.

Another important concern for this study is whether the functions of different cell types could be effectively guided within the 3D nanofibrous multicellular construct. From the cytoskeleton developments of the cells within the constructs over different incubation times (Fig. 4b and 4c), it could be observed that both two types of cells could well attach, stretch, and form cell-cell junctions within the construct layers, providing the basis for sufficient cell-cell interactions [50]. From the different cytoskeleton developments between the ECs and SMCs at different layers of the constructs (Fig. 4d and 4h), it could be verified significant guiding effects of the topography-mediated biomechanical cues endowed by the different structures of the supportive nanofibrous layers. According to the different proliferative rates of the cells within the layers with or without sustained release of growth factors (Fig. 4g and 4f), it could be revealed that the loading and sustained release of growth factors have substantial effects on cellular behavior and functions by offering specific biochemical cues. Comprehensively, the biomimetic 3D nanofibrous multicellular constructs could not only mimic the anatomical structures of blood vessels but also resemble the cell-cell and cell-ECM interactions.

Moreover, not limited to forming the tissue analogues of blood vessels demonstrated in the proof-of-concept study, the concurrent biomanufacturing approach also holds high promise for making a range of functional tissue analogues with the use of other cells, growth factors and biodegradable polymers and with modification(s) of the presented fabrication methodology/procedure. Frankly, for the ease of imaging and monitoring the behaviors and functions of cells within the constructs, we did not prepare the constructs (with an overall thickness of about 200 μm) as thick as the blood vessel wall of a human's artery (about 1 mm) in the current study. But it will be expected to be realized by simply increasing the duration of manufacturing or reducing the compression effects by the electrostatic repulsion during the high-voltage manufacturing process through alternately performing the cell electrospinning/coaxial cell electrospraying using different types of power supplies [37]. In the future investigations, we will further evaluate the interactions among different types of cells in the biomimetic 3D nanofibrous constructs with thicker structures. Although the current investigation has demonstrated the feasibility of preserving cell viability and functions (cytoskeleton developments and proliferation) in the biomimetic 3D nanofibrous multicellular constructs in vitro, in vivo biological performances of the constructs will also be evaluated using animal models, while the choices of cells must meet higher requirements for avoiding the potential immune rejection responses of hosts to the cellularized constructs [51]. For clinical applications in the future, the interfacial stability will be an additional key factor that can affect reliable functions of the biomanufactured constructs. Conventional surgical suturing is an option but it may bring about problems such as secondary injuries to surrounding tissues and/or harms to the incorporated cells. Recently, we have reported a bio-adaptive interfacial material that enabled sutureless bio-integration with blood vessels via instant and stable underwater bio-adhesion [52]. Through coupling of bio-adaptive interfacial materials, the biomanufactured constructs may be integrated with blood vessels, attaining the desired interfacial stability in a sutureless manner.

5. Conclusions

In the current investigation, to produce 3D biomimetic nanofibrous multicellular constructs, a biomanufacturing approach through concurrent emulsion electrospinning and coaxial cell electrospraying was developed and the products were characterized and assessed. It was shown that ECs and SMCs could be incorporated in different construct layers with different arrangements of nanofibers (randomly oriented or aligned) and different encapsulated growth factors (VEGF or PDGF). Both ECs and SMCs had well-preserved cell viability (> 95%) and high density of incorporated cells (> 4×10^5 cells/cm^2) throughout the biomanufacturing process. In 3D nanofibrous multicellular constructs, the different nanofiber arrangements and sequential release of multiple growth factors could guide cell morphology, promote cytoskeleton development, and enhance proliferative activities of incorporated ECs and SMCs. Modelled on the anatomies of blood vessels, the 3D nanofibrous multicellular constructs formed by our biomanufacturing approach resembled the natural cell-cell and cell-ECM organizations and interactions. This biomanufacturing approach holds the promise for not only making functional tissue analogues of blood vessels but also fabricating other functional tissue analogues for diverse tissue engineering and drug screening applications.

CRediT authorship contribution statement

Y. Zhou and Q. Zhao contributed equally to this work. M. Wang conceived and supervised the study. M. Wang and Q. Zhao drafted and revised the manuscript. Y. Zhou and Q. Zhao collected and analyzed the experimental and statistical data.

Declaration of Competing Interest

The authors declare that they have no known competing financial interests or personal relationships that could have appeared to influence the work reported in this paper.

Data Availability

Data will be made available on request.

Acknowledgements

This work was supported by research grants (HKU 7177/13E, 17201017, 17200519 and N_HKU749/22) from the Research Grants Council (RGC) of Hong Kong, research grants from The University of Hong Kong, National Natural Science Foundation of China (52173148, 51903245), the National Natural Science Foundation of China/RGC Joint Research Scheme (52261160380), Youth Innovation Promotion Association of CAS (2022368), and Natural Science Foundation of Guangdong Province (2114050001067). M. Wang thanks a donor in Hong Kong for her generous donation to support his research in biomaterials and tissue engineering at HKU.

Authors' contributions

M. Wang conceived and supervised the study. Y. Zhou and Q. Zhao collected and analyzed the experimental and statistical data. M. Wang and Q. Zhao drafted and revised the manuscript.

References

[1] K.J. Wolf, J.D. Weiss, S.G.M. Uzel, M.A. Skylar-Scott, J.A. Lewis, Biomanufacturing human tissues via organ building blocks, Cell Stem Cell 29 (5) (2022) 667–677.
[2] R.Z. Zhuang, R. Lock, B. Liu, G. Vunjak-Novakovic, Opportunities and challenges in cardiac tissue engineering from an analysis of two decades of advances, Nat. Biomed. Eng. 6 (4) (2022) 327–338.
[3] Y.S. Zhang, G. Haghiashtiani, T. Hübscher, D.J. Kelly, J.M. Lee, M. Lutolf, M. C. McAlpine, W.Y. Yeong, M. Zenobi-Wong, J. Malda, 3D extrusion bioprinting, Nat. Rev. Methods Prim. 1 (2021) 75.
[4] X. Wang, B. Ding, B. Li, Biomimetic electrospun nanofibrous structures for tissue engineering, Mater. Today 16 (6) (2013) 229–241.
[5] J. Ding, J. Zhang, J. Li, D. Li, C. Xiao, H. Xiao, H. Yang, X. Zhuang, X. Chen, Electrospun polymer biomaterials, Prog. Polym. Sci. 90 (2019) 1–34.
[6] A. Shapira, T. Dvir, 3D tissue and organ printing-hope and reality, Adv. Sci. 8 (10) (2021), 2003751.
[7] R. Levato, T. Jungst, R.G. Scheuring, T. Blunk, J. Groll, J. Malda, From shape to function: the next step in bioprinting, Adv. Mater. 32 (12) (2020), 1906423.
[8] A.M. Jorgensen, J.J. Yoo, A. Atala, Solid organ bioprinting: strategies to achieve organ function, Chem. Rev. 120 (19) (2020) 11093–11127.
[9] M. Zhang, R.C. Lin, X. Wang, J.M. Xue, C.J. Deng, C. Feng, H. Zhuang, J.G. Ma, C. Qin, L. Wan, J. Chang, C.T. Wu, 3D printing of Haversian bone-mimicking scaffolds for multicellular delivery in bone regeneration, Sci. Adv. 6 (12) (2020).
[10] W. Liu, Y.S. Zhang, M.A. Heinrich, F. De Ferrari, H.L. Jang, S.M. Bakht, M. M. Alvarez, J. Yang, Y.C. Li, G. Trujillo-de Santiago, A.K. Miri, K. Zhu, P. Khoshakhlagh, G. Prakash, H. Cheng, X. Guan, Z. Zhong, J. Ju, G.H. Zhu, X. Jin, S.R. Shin, M.R. Dokmeci, A. Khademhosseini, Rapid continuous multimaterial extrusion bioprinting, Adv. Mater. 29 (3) (2017), 1604630.
[11] A. Lee, A.R. Hudson, D.J. Shiwarski, J.W. Tashman, T.J. Hinton, S. Yerneni, J. M. Bliley, P.G. Campbell, A.W. Feinberg, 3D bioprinting of collagen to rebuild components of the human heart, Science 365 (6452) (2019) 482–487.
[12] T.H. Qazi, M.R. Blatchley, M.D. Davidson, F.M. Yavitt, M.E. Cooke, K.S. Anseth, J. A. Burdick, Programming hydrogels to probe spatiotemporal cell biology, Cell Stem Cell 29 (5) (2022) 678–691.
[13] J.J. Rice, M.M. Martino, L. De Laporte, F. Tortelli, P.S. Briquez, J.A. Hubbell, Engineering the regenerative microenvironment with biomaterials, Adv. Healthc. Mater. 2 (1) (2013) 57–71.
[14] L.E. Bertassoni, Bioprinting of complex multicellular organs with advanced functionality-recent progress and challenges ahead, Adv. Mater. 34 (3) (2022), 2101321.
[15] J. Xue, T. Wu, Y. Dai, Y. Xia, Electrospinning and electrospun nanofibers: methods, materials, and applications, Chem. Rev. 119 (8) (2019) 5298–5415.
[16] Q. Zhao, H. Cui, J. Wang, H. Chen, Y. Wang, L. Zhang, X. Du, M. Wang, Regulation effects of biomimetic hybrid scaffolds on vascular endothelium remodeling, ACS Appl. Mater. Interfaces 10 (28) (2018) 23583–23594.
[17] A.J. Robinson, A. Perez-Nava, S.C. Ali, J.B. Gonzalez-Campos, J.L. Holloway, E. M. Cosgriff-Hernandez, Comparative analysis of fiber alignment methods in electrospinning, Matter 4 (3) (2021) 821–844.
[18] J. Han, L. Xiong, X. Jiang, X. Yuan, Y. Zhao, D. Yang, Bio-functional electrospun nanomaterials: From topology design to biological applications, Prog. Polym. Sci. 91 (2019) 1–28.
[19] C. Vaquette, J.J. Cooper-White, Increasing electrospun scaffold pore size with tailored collectors for improved cell penetration, Acta Biomater. 7 (6) (2011) 2544–2557.
[20] M. Yeo, G.H. Kim, Anisotropically aligned cell-laden nanofibrous bundle fabricated via cell electrospinning to regenerate skeletal muscle tissue, Small 14 (48) (2018), 1803491.
[21] A.S. Qayyum, E. Jain, G. Kolar, Y. Kim, S.A. Sell, S.P. Zustiak, Design of electrohydrodynamic sprayed polyethylene glycol hydrogel microspheres for cell encapsulation, Biofabrication 9 (2) (2017), 025019.
[22] S.N. Jayasinghe, J. Auguste, C.J. Scotton, Platform technologies for directly reconstructing 3D living biomaterials, Adv. Mater. 27 (47) (2015) 7794–7799.
[23] H. Wang, Y. Yang, J. Liu, L. Qian, Direct cell reprogramming: approaches, mechanisms and progress, Nat. Rev. Mol. Cell Biol. 22 (6) (2021) 410–424.
[24] A.K. Gaharwar, I. Singh, A. Khademhosseini, Engineered biomaterials for in situ tissue regeneration, Nat. Rev. Mater. 5 (9) (2020) 686–705.
[25] Q. Zhao, J. Wang, Y. Wang, H. Cui, X. Du, A stage-specific cell-manipulation platform for inducing endothelialization on demand, Natl. Sci. Rev. 7 (3) (2020) 629–643.
[26] T.D. Stocco, M.C. Moreira Silva, M.A.F. Corat, G. Goncalves Lima, A.O. Lobo, Towards bioinspired meniscus-regenerative scaffolds: engineering a novel 3D bioprinted patient-specific construct reinforced by biomimetically aligned nanofibers, Int. J. Nanomed. 17 (2022) 1111–1124.
[27] M. Yeo, G. Kim, Micro/nano-hierarchical scaffold fabricated using a cell electrospinning/3D printing process for co-culturing myoblasts and HUVECs to induce myoblast alignment and differentiation, Acta Biomater. 107 (2020) 102–114.
[28] A.C. Daly, M.D. Davidson, J.A. Burdick, 3D bioprinting of high cell-density heterogeneous tissue models through spheroid fusion within self-healing hydrogels, Nat. Commun. 12 (1) (2021) 753.
[29] J.A. Brassard, M. Nikolaev, T. Hubscher, M. Hofer, M.P. Lutolf, Recapitulating macro-scale tissue self-organization through organoid bioprinting, Nat. Mater. 20 (1) (2021) 22–29.
[30] H. Zhang, Y. Cong, A.R. Osi, Y. Zhou, F. Huang, R.P. Zaccaria, J. Chen, R. Wang, J. Fu, Direct 3D printed biomimetic scaffolds based on hydrogel microparticles for cell spheroid growth, Adv. Funct. Mater. 30 (13) (2020), 1910573.
[31] S.J. Xin, K.A. Deo, J. Dai, N.K.R. Pandian, D. Chimene, R.M. Moebius, A. Jain, A. Han, A.K. Gaharwar, D.L. Alge, Generalizing hydrogel microparticles into a new class of bioinks for extrusion bioprinting, Sci. Adv. 7 (42) (2021), eabk3087.
[32] Q. Zhao, Y. Zhou, M. Wang, Three-dimensional endothelial cell incorporation within bioactive nanofibrous scaffolds through concurrent emulsion electrospinning and coaxial cell electrospraying, Acta Biomater. 123 (2021) 312–324.
[33] S. Fleischer, D.N. Tavakol, G. Vunjak-Novakovic, From arteries to capillaries: approaches to engineering human vasculature, Adv. Funct. Mater. 30 (37) (2020), 1910811.
[34] C. Souilhol, J. Serbanovic-Canic, M. Fragiadaki, T.J. Chico, V. Ridger, H. Roddie, P. C. Evans, Endothelial responses to shear stress in atherosclerosis: a novel role for developmental genes, Nat. Rev. Cardiol. 17 (1) (2020) 52–63.
[35] S. Hauser, F. Jung, J. Pietzsch, Human endothelial cell models in biomaterial research, Trends Biotechnol. 35 (3) (2017) 265–277.
[36] S. Cheng, Y. Jin, N. Wang, F. Cao, W. Zhang, W. Bai, W. Zheng, X. Jiang, Self-adjusting, polymeric multilayered roll that can keep the shapes of the blood vessel scaffolds during biodegradation, Adv. Mater. 29 (28) (2017), 1700171.
[37] H.-W. Tong, M. Wang, Electrospinning of poly(hydroxybutyrate-co-hydroxyvalerate) fibrous tissue engineering scaffolds in two different electric fields, Polym. Eng. Sci. 51 (7) (2011) 1325–1338.
[38] S.J. Dixon, B.R. Stockwell, The role of iron and reactive oxygen species in cell death, Nat. Chem. Biol. 10 (1) (2014) 9–17.
[39] M.P. Lutolf, J.A. Hubbell, Synthetic biomaterials as instructive extracellular microenvironments for morphogenesis in tissue engineering, Nat. Biotechnol. 23 (1) (2005) 47–55.
[40] R.G. Wylie, S. Ahsan, Y. Aizawa, K.L. Maxwell, C.M. Morshead, M.S. Shoichet, Spatially controlled simultaneous patterning of multiple growth factors in three-dimensional hydrogels, Nat. Mater. 10 (10) (2011) 799–806.
[41] E.S. Place, N.D. Evans, M.M. Stevens, Complexity in biomaterials for tissue engineering, Nat. Mater. 8 (6) (2009) 457–470.
[42] Y. Zhou, Q. Zhao, M. Wang, Dual release of VEGF and PDGF from emulsion electrospun bilayer scaffolds consisting of orthogonally aligned nanofibers for gastrointestinal tract regeneration, MRS Commun. 9 (03) (2019) 1098–1104.
[43] K. Wei, Y. Li, X. Lei, H. Yang, A. Teramoto, J. Yao, K. Abe, F.K. Ko, Emulsion electrospinning of a collagen-like protein/PLGA fibrous scaffold: empirical modeling and preliminary release assessment of encapsulated protein, Macromol. Biosci. 11 (11) (2011) 1526–1536.
[44] I. Zachary, VEGF signalling: integration and multi-tasking in endothelial cell biology, Biochem. Soc. Trans. 31 (6) (2003) 1171–1177.
[45] Q. Zhao, J. Wang, H. Cui, H. Chen, Y. Wang, X. Du, Programmed shape-morphing scaffolds enabling facile 3D endothelialization, Adv. Funct. Mater. 28 (29) (2018), 1801027.
[46] M.D. Tallquist, W.J. French, P. Soriano, Additive effects of PDGF receptor β signaling pathways in vascular smooth muscle cell development, PLoS Biol. 1 (2) (2003), e52.
[47] G.L. Basatemur, H.F. Jorgensen, M.C.H. Clarke, M.R. Bennett, Z. Mallat, Vascular smooth muscle cells in atherosclerosis, Nat. Rev. Cardiol. 16 (12) (2019) 727–744.
[48] S. Weinbaum, J.M. Tarbell, E.R. Damiano, The structure and function of the endothelial glycocalyx layer, Annu. Rev. Biomed. Eng. 9 (2007) 121–167.
[49] Q. Zhao, W.W. Lu, M. Wang, Modulating the release of vascular endothelial growth factor by negative-voltage emulsion electrospinning for improved vascular regeneration, Mater. Lett. 193 (2017) 1–4.
[50] E. Dejana, Endothelial cell–cell junctions: happy together, Nat. Rev. Mol. Cell Biol. 5 (4) (2004) 261–270.
[51] A. Fayon, P. Menu, R. El Omar, Cellularized small-caliber tissue-engineered vascular grafts: looking for the ultimate gold standard, NPJ Regen. Med. 6 (1) (2021) 1–11.
[52] S. Wang, Q. Zhao, J. Li, X. Du, Morphing-to-adhesion polysaccharide hydrogel for adaptive biointerfaces, ACS Appl. Mater. Interfaces 14 (37) (2022) 42420–42429.